Review Article

Kozo Fujiwara*, Lu-Chung Chuang, and Kensaku Maeda

Dynamics at crystal/melt interface during solidification of multicrystalline silicon

https://doi.org/10.1515/htmp-2022-0020
received September 24, 2021; accepted December 06, 2021

Abstract: A fundamental understanding of crystal growth dynamics during directional solidification of multicrystalline Si (mc-Si) is crucial for the development of crystal growth technology for mc-Si ingots for use in solar cells. *In situ* observation of the crystal/melt interface is a way to obtain direct evidence of phenomena that occur at a moving crystal/melt interface during growth. In this review, some of the phenomena occurring in the solidification processes of mc-Si are introduced based on our *in situ* observation experiments, after a brief introduction of the history of the development of crystal growth technologies to obtain mc-Si ingots for solar cells.

Keywords: solidification, crystal/melt interface, semiconductor, grain boundary

1 Introduction

To solve the problem of global warming, decarbonization policies are being promoted all over the world, and it is expected that the use of solar power generation will further expand in the future. Recently, solar cells using various materials such as perovskites are being actively researched; but in practice, crystalline Si solar cells accounted for about 95% of the total solar cell production in 2019 [1]. Considering manufacturing cost, safety, reliability, and abundance of resources, crystalline Si solar cells are expected to continue to be the main product in the future. Single-crystal Si (mono-Si) and multicrystalline Si (mc-Si) are used as substrate materials for crystalline Si solar cells, and recently the production of mono-Si solar cells has been increasing owing to a decrease in the production cost of mono-Si ingots grown by the Czochralski (CZ) method [1]. However, comparing the weight of the ingot, mc-Si ingots grown by directional solidification in a crucible are four to five times larger than mono-Si ingots grown by the CZ method [1]. Therefore, in the future, if the quality of mc-Si ingots is improved further, their use may increase again. Control of the "grain structure" in mc-Si ingots, which contain not only a distribution of grain sizes and grain orientations but also a distribution in the density of crystal defects, is the key for improving their quality. For the development of crystal growth technology for mc-Si ingots, a fundamental understanding of the crystal growth mechanisms is crucial.

In this review, first, the history of the growth technology for mc-Si ingots is briefly described, and then some of the phenomena that occur during the directional solidification process will be explained based on the results of our *in situ* observation experiments.

2 Growth of mc-Si ingots for solar cells

The following is a brief introduction to the history of the development of the growth technology for mc-Si ingots. Research on the directional solidification of mc-Si ingots for solar cells began in earnest in the late 1970s. Carbon (graphite) or silica crucibles were used for the directional solidification of mc-Si ingots [2–10]. Because a silicon melt is very reactive toward the crucible materials, silicon nitride powders were used to coat the inside wall of the crucible as a mold release agent to prevent sticking and cracking of the ingot [3]. Silicon nitride-coated crucibles are commonly used for the growth of mc-Si ingots at present. In earlier research, the purity of the Si feedstock was not high, so the conversion efficiency of solar cells based on mc-Si substrates was around 15% in the 1980s [11]. The purity of Si feedstock has been improved [12,13],

* **Corresponding author: Kozo Fujiwara,** Institute for Materials Research, Tohoku University, Sendai, 980-8577, Japan, e-mail: kozo@imr.tohoku.ac.jp
Lu-Chung Chuang, Kensaku Maeda: Institute for Materials Research, Tohoku University, Sendai, 980-8577, Japan

Open Access. © 2022 Kozo Fujiwara *et al.*, published by De Gruyter. This work is licensed under the Creative Commons Attribution 4.0 International License.

and a stable supply of high-purity feedstock is available for the growth of mc-Si; thus, the energy conversion efficiency of mc-Si solar cells has been improved.

Owing to numerous studies, it has been recognized that various types of crystal defects in mc-Si ingots, such as metallic impurities, dislocation clusters, and grain boundaries, degrade the properties of solar cells [14–42] because they act as recombination centers for photo-carriers. Therefore, a decrease in the defect density of mc-Si ingots has been demanded, and new growth methods for controlling the "grain structure" of mc-Si ingots have been proposed and developed. Here, a few of them are introduced. Commonly, in the growth of mc-Si ingots, nucleation of crystal grains occurs on the bottom wall of the crucible. The impingement of grains forms the initial grain structure of the mc-Si ingot, and then the ingot is directionally grown toward the upper side, as schematically shown in Figure 1(a). In 2006, the "dendritic casting method" was proposed where dendrite growth is promoted along the bottom wall of the crucible in the early stage of directional solidification, as shown in Figure 1(b) [43,44]. Because the growth rate of the dendrite grains is much faster than that of normal crystal grains [43,45,46], a grain structure with larger crystal grains is formed at the bottom of the ingot. This structure formed on the bottom wall of the crucible will act as a "seed" for the following directional solidification. Around the same time, BP Solar developed the "mono casting method" where a single crystal seed is placed on the bottom of the crucible in advance; thus, a mono-Si ingot would be grown by directional solidification from the seed, as shown in Figure 1(c) [47]. Methods that use several seed set on the bottom of the crucible have been developed [48–51], which were derived from the mono casting method. Also, a method that involves seeding from the top of the melt in the crucible has been studied to promote crystallization inside the melt [52–54]. In the dendritic-casting and seed-assisted growth methods, the aim is to obtain a grain structure with larger crystal grains to reduce the grain boundary density. However, Lan's group proposed mc-Si ingots with smaller crystal grains and showed that the minority carrier lifetime was improved compared with that of mc-Si with larger grains [55,56]. This was mainly due to the reduction of dislocation clusters in the grains; the large number of random grain boundaries may have served as sinks for dislocation clusters in the solidification of these mc-Si ingots. The mc-Si ingots with smaller crystal grains are referred to as "high performance (HP) mc-Si." In the growth of HP mc-Si ingots, tiny beads (Si, SiO_2, or other materials) are set on the bottom of the crucible to increase the nucleation sites at the beginning of solidification, which leads to the formation of a grain structure with smaller grains, as shown in Figure 1(d). At present, HP mc-Si is widely used

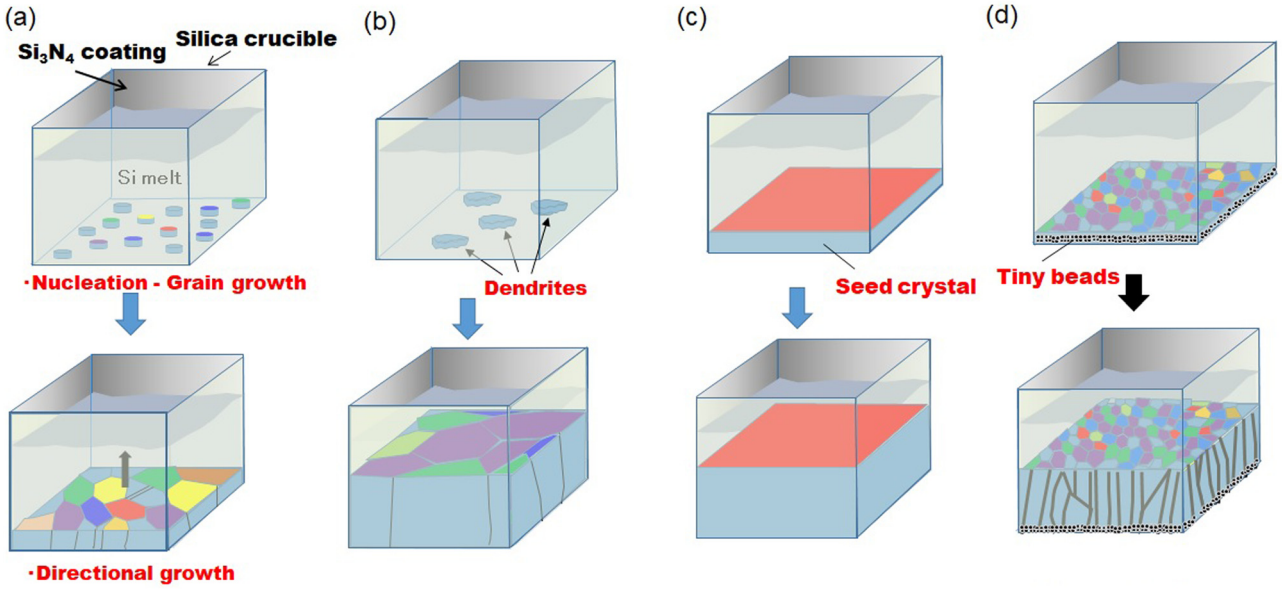

Figure 1: Directional solidification processes in various methods for producing mc-Si ingots for solar cells: (a) conventional directional solidification method, (b) dendritic casting method, where dendrite growth is promoted along the bottom wall of the crucible to create a grain structure with large grains, (c) mono casting method, where a single crystal is preset on the bottom wall of the crucible to grow a single crystal ingot in the crucible, and (d) HP mc-Si growth, where tiny beads are preset on the bottom wall of the crucible to enhance nucleation to obtain a grain structure with small grains.

commercially. The energy conversion efficiency of solar cells based on HP mc-Si has reached more than 19% [57–59]. The development efforts for each growth method, especially regarding the recent development of seed-assisted growth, are reviewed well in ref. [60].

As outlined above, control of the grain structure in the solidification process of mc-Si is the key for obtaining high quality ingots. Usually, the bottom structure will not be maintained at the top of the ingot, because the microstructure continuously changes during directional solidification. To control the microstructure during directional solidification, it is crucial to understand the fundamental phenomena that occur during the solidification processes. In the next section, some of these phenomena will be explained.

3 Crystal growth dynamics in solidification processes of mc-Si ingots

3.1 *In situ* observation system

In our earliest study on observing the solidification processes of Si [61], we used a confocal scanning laser microscope with an infrared image furnace, which had been established for observing solidification processes in iron/steel materials [62,63]. In that system, the available sample size was limited in a few millimeters and a ceramic crucible was used. So that we can observe various phenomena that occur in the solidification processes of Si, we developed an *in situ* observation system which consists of an optical digital microscope and a growth furnace, as shown in Figure 2 [64,65]. In this system, we usually use a silica crucible with a size of 22 mm × 12 mm × 11 mm. The upper surface of the sample is observed through a silica window on the upper part of the furnace. The temperature inside the furnace is controlled by two carbon heaters, and the temperature gradient can be controlled by controlling the power output of the heaters. When we would like to observe a crystal/melt interface during directional solidification, crystal growth can be initiated from one side of the crucible by controlling the temperatures of the two carbon heaters.

Another method for observing the crystal/melt interface of Si has been developed, the X-ray imaging method, which is also a powerful tool for fundamental studies on mc-Si [66–70].

3.2 Growth shape of crystal grains

At the beginning of directional solidification without any seed crystals, nucleation and growth of the crystal grains occur on the bottom wall of the crucible, as shown in Figure 1(a). During grain growth of the nuclei, the shape of the crystal is determined by the anisotropy of the growth rate among crystallographic planes; that shape is called the “growth shape,” whereas the “equilibrium shape” of a crystal grain is determined by minimization of the crystal/melt interfacial energy under constant volume [71,72]. Observation of the equilibrium shape of Si in the melt was attempted experimentally [73], and it has been investigated using simulations [74–76]. Figure 3 shows the typical growth shapes of Si crystal grains with different upper orientations [73,77]. Because the growth rate of {111} planes is the lowest, the growth shape is bounded by {111} planes, as schematically shown in Figure 3. Therefore, the

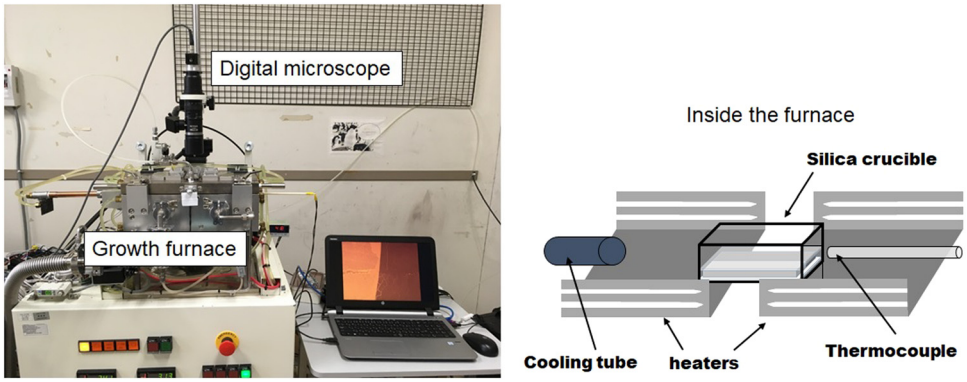

Figure 2: *In situ* observation system consisting of a crystal growth furnace and a digital optical microscope: (left) picture of the system and (right) schematic image of the inside of the furnace.

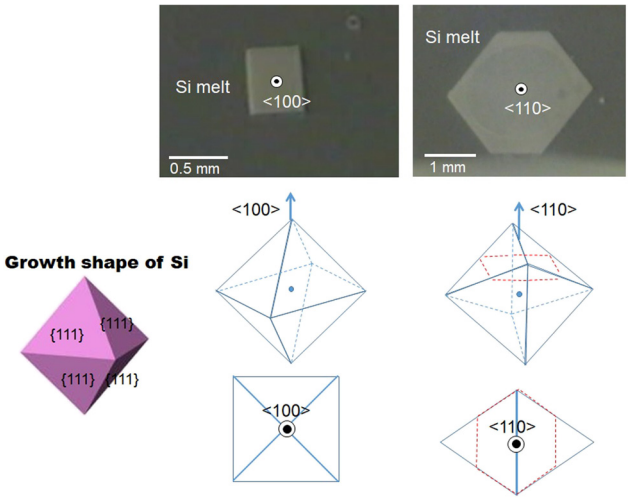

Figure 3: Growth shape for a normal Si crystal with different upper orientations. The shape is bounded by {111} planes because they have the lowest growth rate [73,77].

observed shape of the crystals on the crucible wall is determined by the crystallographic orientation in the upper direction, as seen in Figure 3.

However, the dendritic growth often appears in Si melts even at low undercooling [45,78]. When a Si crystal (or nucleus) contains parallel twin boundaries [79], the crystal grows in a dendritic shape, as shown in Figure 4. This is a so-called "faceted dendrite." The growth shape and the growth mechanism of a faceted dendrite are very different from the dendrites of metallic alloys. The Si-faceted dendrite contains at least two parallel twin boundaries at the center and, preferentially, grows in the <112> or <110> direction, which is determined by the growth mechanism related to the formation of reentrant corners at the growth front of the faceted dendrite. The details of the growth mechanism of a faceted dendrite are given in earlier studies [80,81].

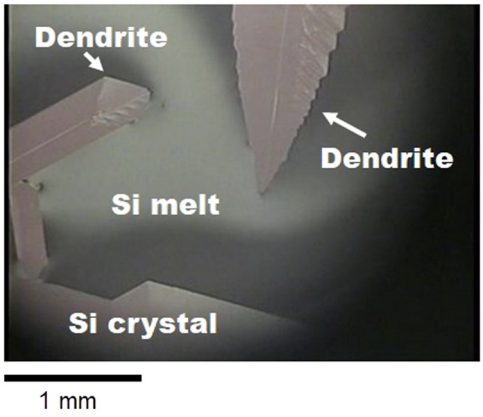

Figure 4: Dendrites growing in the Si melt.

Such faceted dendrite growth was also directly observed for the compound semiconductor GaSb, and it was found that its growth mechanism is similar to that of Si [82]. The growth rate of the faceted dendrites is much higher than that of normal crystal grains, and thus the grain size becomes larger when dendrite growth is promoted along the bottom wall of the crucible in the early stage of directional solidification, which is the basic idea behind the dendritic casting method [43]. However, in HP mc-Si, the grain size must be kept small and homogeneous. To realize that grain structure, the nucleation frequency in the early stage of solidification must be increased. To enhance the number of nucleation events, tiny Si (or other materials) beads are preset on the bottom wall of the crucible [55–59], as show in Figure 1(d).

3.3 Morphology of crystal/melt interface

During the directional growth process of the mc-Si ingot, it is significant to control the entire interface shape, as shown in Figure 5(a), because it influences on the distribution of thermal stress and the defect density in an entire ingot. To control the entire interface shape macroscopically, not only the temperature gradient in the furnace and the growth rate but also the shape of the crucible and the furnace design should be considered. One can refer to other literature for details on control of the macroscopic crystal/melt interface shape [83–89].

Here, we would prefer to consider the microscopic (submillimeter scale) shape of the crystal/melt interface for Si.

First, we consider the case of a crystal that does not contain grain boundaries (single crystal) [81,90–92]. Even if the interface looks macroscopically flat, it can have a flat or zigzag shape on the microscopic scale, as schematically shown in Figure 5(b). Also, it should be noted that even if the interface shape looks microscopically flat, it may have a rough interface or a smooth interface at the atomic level, as schematically shown in Figure 5(c). In the case of Si, according to Jackson's criteria [93,94], planes other than {111} planes are atomically rough, and only the {111} plane is an atomically smooth "facet plane."

When the plane of the crystal/melt interface is a rough plane, the microscopic interface shape is kept flat under the condition that the degree of undercooling of the melt in front of the crystal/melt interface is smaller than that at the crystal/melt interface. Generally, in the directional solidification process of mc-Si ingots, the temperature gradient in the furnace is positive to the direction of the solidification and the growth rate is low

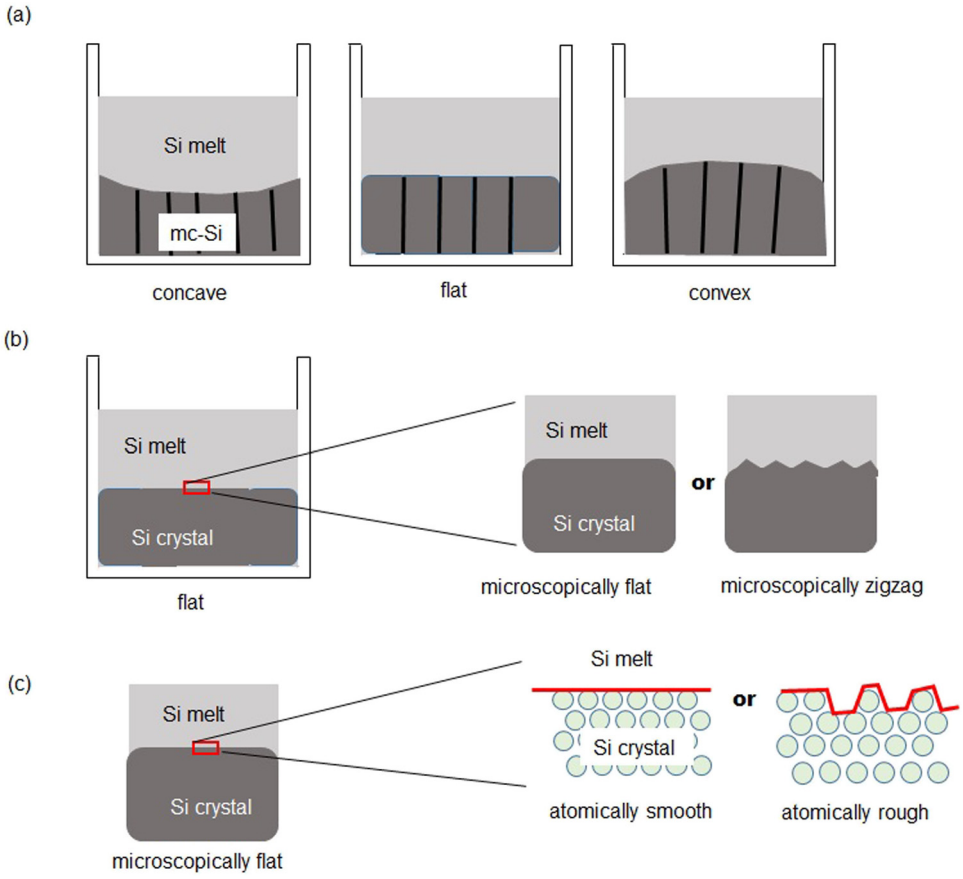

Figure 5: Schematic images of crystal/melt interface shapes on various scales: (a) macroscopic images of concave, flat, and convex-shaped crystal/melt interfaces during directional solidification, (b) microscopic images of flat and zigzag-shaped crystal/melt interfaces, and (c) atomic images of rough and smooth crystal/melt interfaces.

enough, and thus a flat interface would be kept microscopically. If the growth rate increases and the degree of undercooling of the melt becomes larger than that at the crystal/melt interface, the interface shape transforms from flat to zigzag, as schematically shown in Figure 6(a). However, in the case of a facet plane, the microscopic interface shape remains flat even as the growth rate is increased, as shown in Figure 6(b).

The transformation of a flat interface to a zigzag one in a rough plane is known as the Mullins–Sekerka interface instability [95]. This is explained as interface instability that occurs when the temperature gradient in the melt at the crystal/melt interface is negative in the growth direction, as shown in Figure 7. It can be considered that the flat interface is often perturbed during growth, and when perturbation is introduced to a planar interface, the degree of undercooling at the top of the perturbed part is larger than that at the bottom part under a negative temperature gradient, as schematically shown in Figure 7(a). Therefore, the growth rate at the top part is higher than that at the bottom part, which leads to amplification of the perturbation. The amplified perturbed part will be bounded by {111} planes finally in the case of Si because these planes have the lowest growth rate, which is similar to the evolution of the growth shape of crystal grains (see Figure 3). Actually, this transformation from a flat to a perturbed to a zigzag shape has been directly observed, as shown in Figure 7(b). However, when the temperature gradient is positive, the growth rate at the top part of the perturbation is lower than that at the bottom part; therefore, the bottom part will catch up with the top part, and a flat interface is maintained. In the case that the crystal/melt interface is a facet plane, which is the {111} plane of Si, the flat interface is already bounded by the plane with the lowest growth rate, and thus a change of the interface shape does not occur even for a negative temperature gradient, as shown in Figure 6(b).

The critical growth rate where the temperature gradient in the melt changes from positive to negative is dependent on the temperature gradient in the furnace. Here, it should be noted that when the temperature gradient in the furnace is set to be positive, the temperature gradient in the melt can be negative at a higher growth rate due to release of the

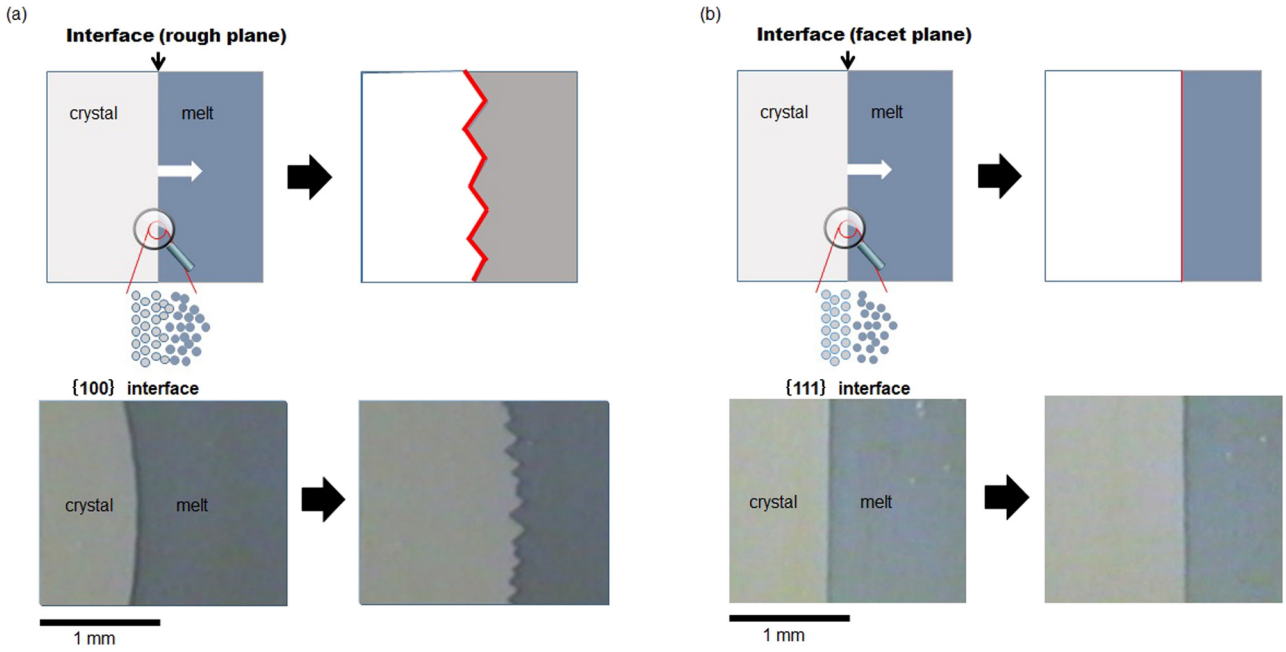

Figure 6: Transformation of microscopic interface shape for atomically rough and smooth planes [90]: (a) the case of a rough plane. The flat interface is transformed to a zigzag interface with increasing growth rate due to the interface instability and (b) the case of a smooth plane (facet plane). The flat interface is maintained even at a higher growth rate.

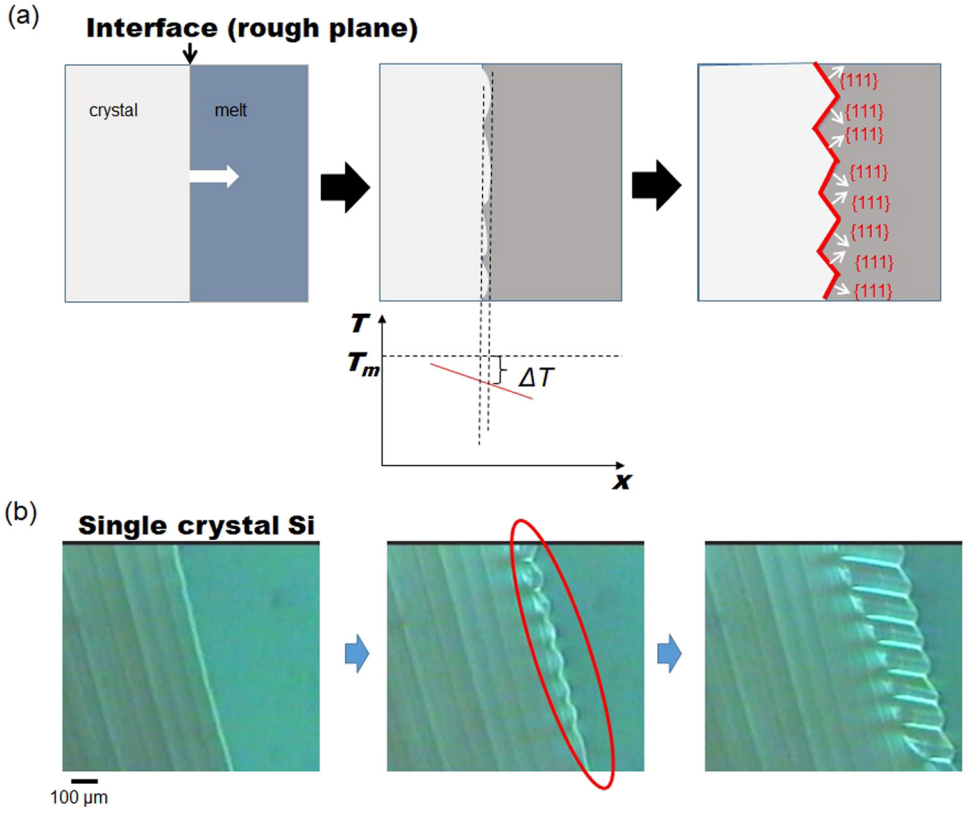

Figure 7: Process of interface instability: (a) schematic image of the interface at the instability with a temperature gradient at the interface. Under a negative temperature gradient, the perturbation introduced into the flat interface is amplified, and a zigzag interface is formed finally and (b) actual images of the interface at the point of interface instability for a Si single crystal.

latent heat of crystallization. In our experimental set-up, the one-dimensional thermal field in the crystal and melt along the crystal growth direction, $T_{c,m}$, can be calculated by equation (1a–c) [90],

$$T_{c,m}(x) = A_{c,m}\exp\left(-\frac{x}{l_{c,m}}\right) + Gx + \frac{\rho_{c,m}C_{p_{c,m}}GVl_q l_{Si}}{k_q} + T_i, \quad (1a)$$

$$l_c = \frac{2}{\rho_c C_{Pc}V/k_c - \sqrt{(\rho_c C_{Pc}V/k_c)^2 + 8k_q/k_c l_q l_{Si}}}, \quad (1b)$$

$$l_m = \frac{2}{\rho_m C_{Pm}V/k_m + \sqrt{(\rho_m C_{Pm}V/k_m)^2 + 8k_q/k_m l_q l_{Si}}}, \quad (1c)$$

where $\rho_{c,m}$, $C_{Pc,m}$, $k_{c,m}$, k_q, l_q, l_{Si}, and V are the heat capacity of the Si crystal and melt, the thermal conductivity of the Si crystal and melt, the thermal conductivity of the quartz plate, the thickness of the quartz plate, the thickness of the Si crystal, and the growth velocity, respectively. G is the temperature gradient in the furnace, and T_i is the furnace temperature at the interface position. $A_{c,m}$ is a constant determined by the boundary conditions: these are energy conservation at the crystal-melt interface described as $\Delta HV = k_c(\partial T_c/\partial x)_{x=0} - k_m(\partial T_m/\partial x)_{x=0}$, where ΔH is the latent heat of Si, and temperature continuity at the crystal-melt interface, which is considered to be at the melting temperature T_{mp}, and thus is described as $(T_c)_{x=0} = (T_m)_{x=0} = T_{mp}$. In the calculations, the values of l_q, l_{Si}, and G are based on our experimental values, and the other physical properties of Si used are based on those reported in an earlier study [96]. The temperature gradient at the crystal/melt interface ($x = 0$), G_0, is defined as follows:

$$G_0 = \left.\frac{\partial T_{c,m}}{\partial x}\right|_{x=0} = -\frac{A_{c,m}}{l_{c,m}} + G. \quad (2)$$

The critical growth rate V_{cri} is defined as the growth rate where the temperature gradient in the melt at the interface changes from positive to negative, which can be calculated from the condition $G_0 = 0$ using equation (2). Figure 8 shows the calculated temperature field for various growth rates [90]. It is shown that when the growth rate is low, the temperature gradient in the melt remains positive, whereas it becomes negative at a high growth rate. The calculated critical growth rate is $V_c = 109\ \mu m{\cdot}s^{-1}$ [90], and the V_c obtained by our *in situ* observations was $100\ \mu m{\cdot}s^{-1} < V_c < 150\ \mu m{\cdot}s^{-1}$ [90,92].

Next, we consider the interface instability for a crystal containing grain boundaries. Figure 9 shows a crystal/melt interface containing (a) a small-angle grain boundary and (b) a Σ3 twin boundary [97]. It is clearly observed that the

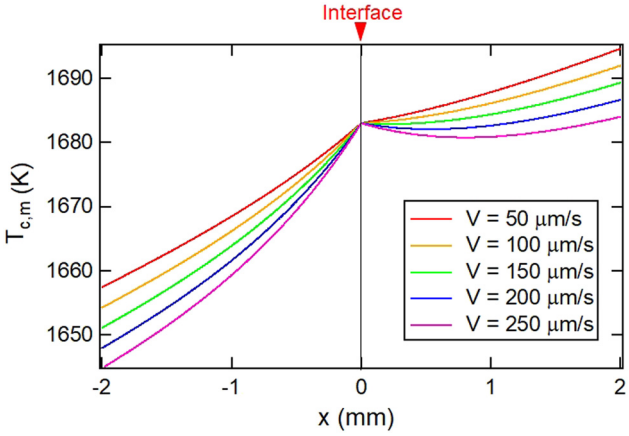

Figure 8: Calculated thermal field in the growth direction at various growth rates [90]. When the growth rate is low, the temperature gradient in the melt at the interface is positive, whereas it becomes negative at a high growth rate. The calculated critical growth rate where the temperature gradient changes from positive to negative is 109 $\mu m{\cdot}s^{-1}$ under our experimental conditions.

instability started at portions of the grain boundary in both cases, whereas the instability began over the entire interface at the same time in the case of single-crystal Si, as shown in Figure 7(b). The critical growth rate for initiation of instability at the grain boundary was found to be smaller than that in the case of a single crystal [97]. It was also shown that the critical growth rate was different depending on the characteristics of the grain boundary, such that $V_R < V_{SAG} < V_{\Sigma 3}$, where V_R, V_{SAG}, and $V_{\Sigma 3}$ are the critical growth rates at a random grain boundary, small-angle grain boundary, and Σ3 twin boundary, respectively [97].

Here, we consider the reason why the interface instability is initiated at a position on a grain boundary. As explained above, the formation of a negative temperature gradient in the melt at the interface causes interface instability. In case of a single crystal, the instability occurs over the entire interface at the same time due to the homogeneous thermal field. However, when a grain boundary exists on the interface, it is considered that the thermal field is locally different around the position of the grain boundary. Factors that affect the thermal field at the crystal/melt interface are the latent heat of crystallization, and diffusion of the generated latent heat from the crystal/melt interface into the crystal and the melt when the temperature gradient in the furnace is fixed. As considered that the crystal imperfections such as grain boundaries affect the electric conduction [98], we can imagine that the thermal conductivity at a grain boundary is lower than that within the grain due to the disordered atomic structure at the grain boundary, as schematically shown in Figure 10. However, the thermal

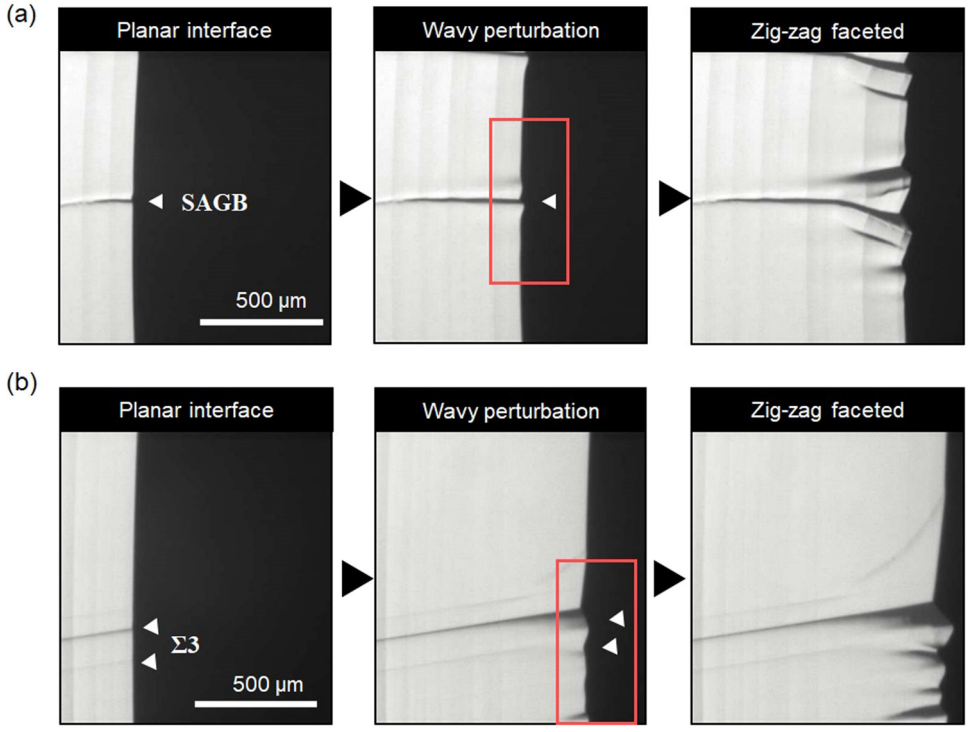

Figure 9: *In situ* observations of interface instability for Si crystals containing grain boundaries [97]: (a) crystal with a small-angle grain boundary and (b) crystal with Σ3 twin boundaries. In both cases, the interface instability was initiated at the grain boundary position.

conductivity in the melt would not be changed even when the crystal contains grain boundaries.

However, to our knowledge, the thermal conductivity at grain boundaries at the melting temperature has not been reported yet. Therefore, we estimated the thermal conductivities at grain boundaries from our *in situ* experiments [97]. As explained above, we can estimate the critical growth rate from equation (2) when all of the physical properties in equation (1a–c) are known. Conversely, when one physical value in equation (1a–c) is unknown and the critical growth rate is obtained by experiment, the unknown value can be calculated. Here, the thermal conductivity at grain boundaries at the melting temperature is unknown, but we can directly measure the critical growth rate at the instability at the grain boundary position [97]. Therefore, it was possible to calculate the thermal conductivity at each grain boundary. However, it should be noted that the width of the "grain boundary area" that affects the thermal field is not known. Therefore, the obtained thermal conductivity might be an "effective" thermal conductivity in the area including a grain boundary. From the *in situ* observations, the critical growth rates of a small-angle grain boundary, Σ3 twin boundary, and random grain boundary were found to be 110, 119, and 37 μm·s^{-1}, respectively [97]. In the case of a single crystal with no grain boundaries, the critical growth rate was 139 μm·s^{-1} [97]. The temperature gradient at the interface G_0 must be zero at the critical growth rate. Therefore, the effective thermal conductivity at each grain boundary is determined so that the $G_0 = 0$ at the critical growth rates by using equation (2). The obtained effective thermal conductivities at the melting temperature were 1.6×10^{-2}, 1.9×10^{-2}, and 2.7×10^{-3} W·K^{-1}·mm^{-1} for small-angle, Σ3, and random grain boundaries, respectively. The thermal conductivity of a single crystal was obtained as 2.2×10^{-2} W·K^{-1}·mm^{-1}. This shows that a negative temperature gradient is locally formed at a portion of the grain boundary due to the lower

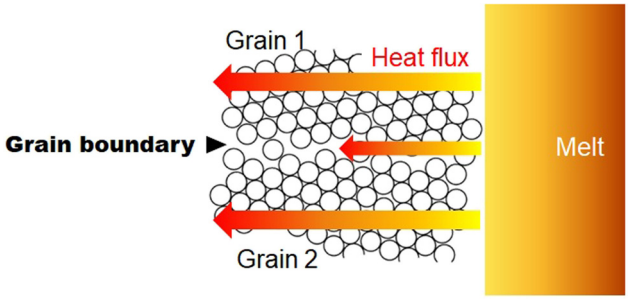

Figure 10: Schematic image of thermal diffusivity at a crystal/melt interface with a grain boundary [97]. The thermal conductivity at the grain boundary is lower than that within the grain due to the disordered atomic configuration.

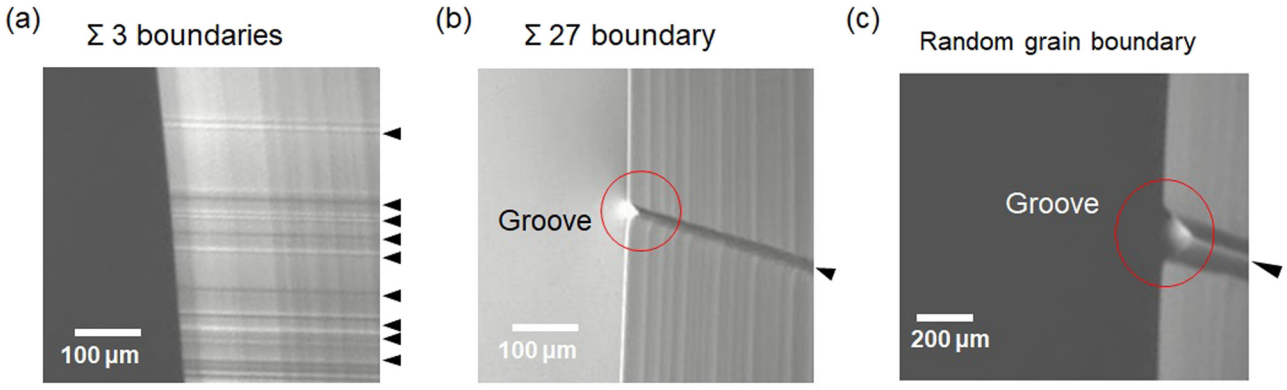

Figure 11: Shape of crystal/melt interfaces for various grain boundary characteristics [100]: (a) an interface with Σ3 twin boundaries. A grain boundary groove is not observed, (b) an interface with a Σ27 grain boundary. A faceted grain boundary groove is observed, and (c) an interface with a random grain boundary. A faceted groove is observed, similar to (b).

thermal conductivity, which promotes the instability at the grain boundary position on the crystal/melt interface.

3.4 Twin boundary formation at the grain boundary groove

In a solidified mc-Si ingot, it is often observed that Σ3{111} twin boundaries are generated from a large-angle grain boundary. Here, we consider the underlying mechanism of twin boundary formation at a grain boundary at a crystal/melt interface. Duffar and Nadri theoretically determined that a {111} facet may appear at the grain boundary groove on the crystal/melt interface, and twin nucleation occurs on the {111} facet at the groove [99]. The shape of the grain boundary groove was observed directly, and a faceted groove was confirmed at grain boundaries other than the Σ3{111} twin boundary, as shown in Figure 11 [100].

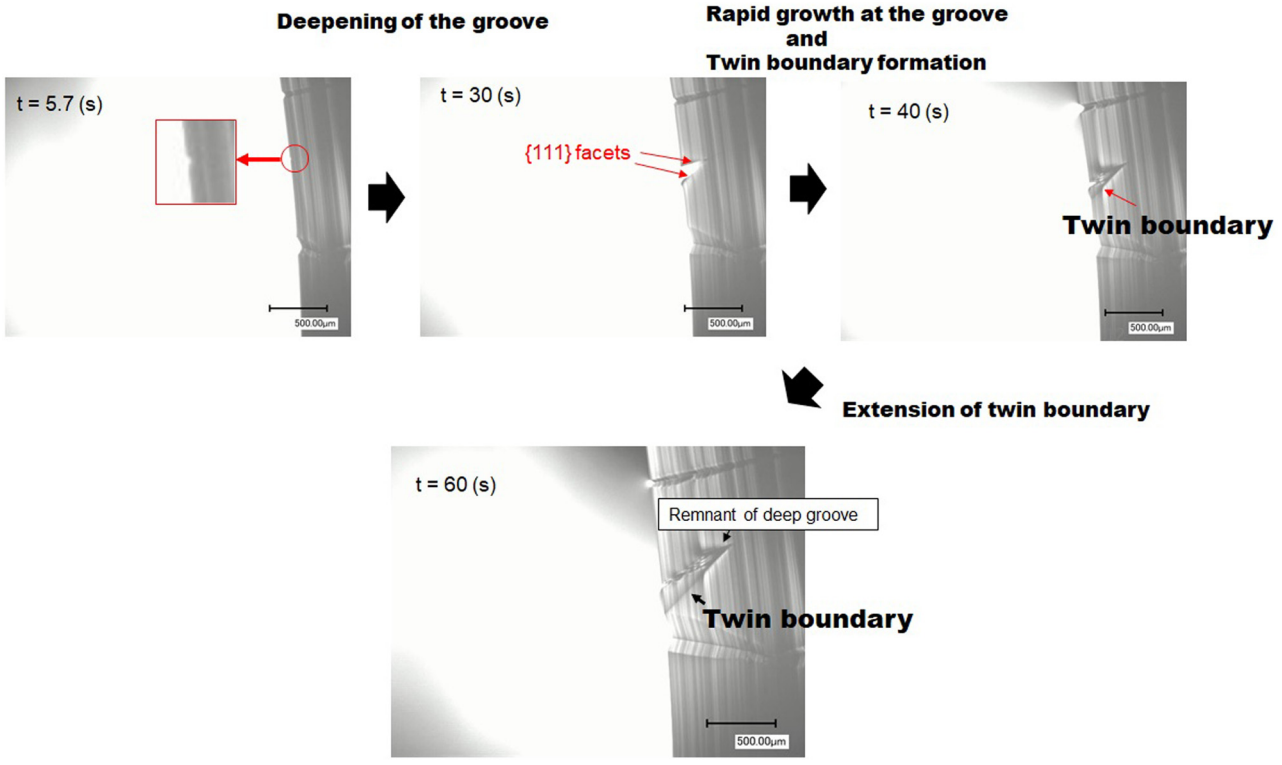

Figure 12: Process of twin boundary formation at a grain boundary groove. When the groove becomes deep enough, rapid growth occurs at the groove, and then twin nucleation occurs on the {111} facet that formed the groove [102].

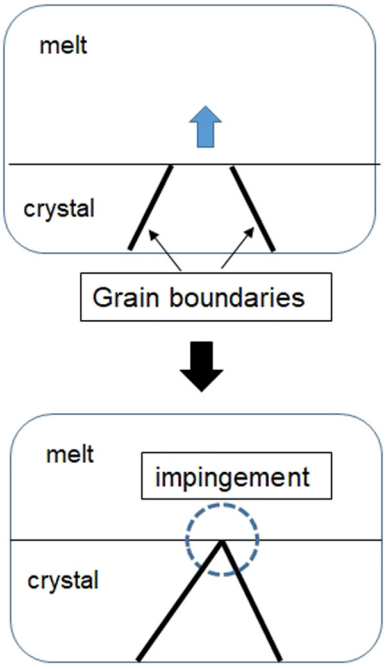

Figure 13: Schematic image of the impingement of two-grain boundaries at a crystal/melt interface.

Tsoutsouva et al. directly observed twin boundary formation at a faceted grain boundary groove by using an *in situ* X-ray imaging method [101], and we also observed this phenomenon directly by our *in situ* observation system [102]. Figure 12 shows the process of twin boundary formation. It is seen that the grain boundary groove indicated by a red circle (t = 5.7 s) was gradually deepened with crystal growth, and the melt inside the groove was rapidly crystallized when the depth of the groove became large enough (between t = 30 and t = 40 s). During this rapid growth to fill the groove, twin nucleation occured on the {111} facet in the groove.

The degree of the driving force (undercooling) for twin nucleation has not been directly obtained experimentally. Theoretical models indicate the probability of twin nucleation as a function of the degree of undercooling, but the value is dependent on the model [99,103,104]. Therefore, further studies are expected in the future.

3.5 Interaction of grain boundaries at the crystal/melt interface

In order to understand the formation of the grain structure of mc-Si during directional solidification, the dynamics of grain boundaries at the crystal/melt interface should be clarified.

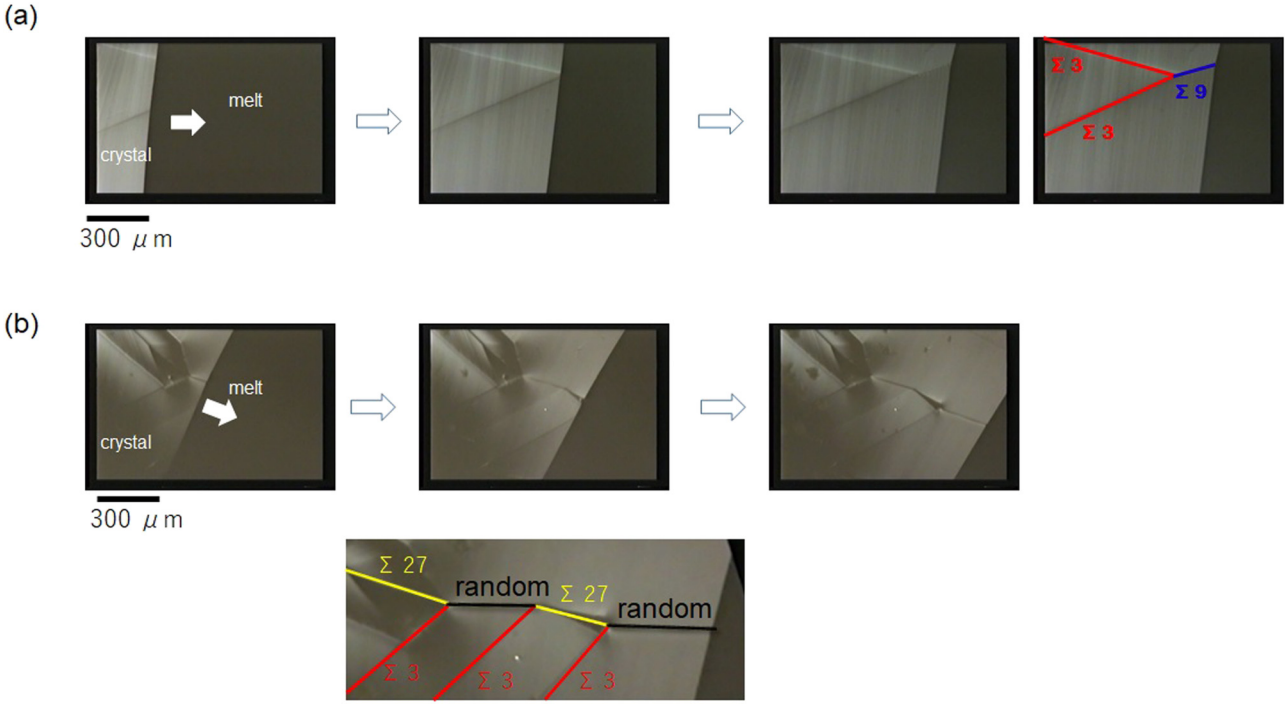

Figure 14: Observations of grain boundary impingement: (a) two Σ3 grain boundaries impinge at the interface, and a Σ9 grain boundary is formed and (b) a Σ27 grain boundary and a Σ3 grain boundary produce a random grain boundary after the impingement, and a random grain boundary and a Σ3 grain boundary produce a Σ27 grain boundary after the impingement.

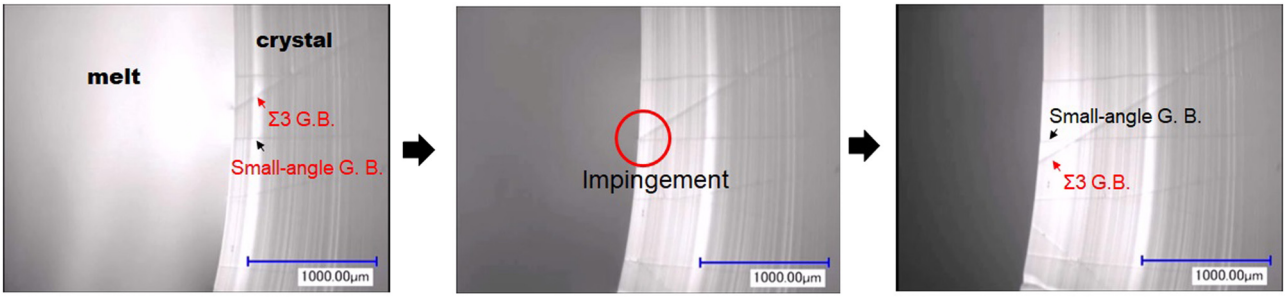

Figure 15: Observations of the impingement of a small-angle grain boundary and a Σ3 twin boundary [112]. The grain boundaries penetrate each other and extend with growth.

In earlier works on grain growth at the crystal/melt interface during directional solidification, the grain growth behavior was discussed on the basis of the difference in the crystal/melt interfacial energy between two adjacent grains [65]. However, recent studies indicated that grain growth at a crystal/melt interface is affected by the kinetics at a grain boundary groove. The direction of extension for the grain boundary has been investigated theoretically [105] and by experiment [106,107], focusing on the shape and growth rate at a grain boundary groove. Those studies showed that the direction of extension for a grain boundary is determined by the difference in the growth rates of two facet planes forming a grain boundary groove. When two facet planes grow with the same growth rate, the grain boundary extends along the bisector line of the groove, and when the growth rates of two facet planes are different, the grain boundary extends in the direction of the sum of the growth rate vectors [107].

Also, the formation of small-angle grain boundaries (SAGB) was directly observed at a moving crystal/melt interface due to the aggregation of dislocations during directional solidification [108,109].

Further, in the directional solidification of mc-Si, two-grain boundaries are often encountered at a crystal/melt interface, as schematically shown in Figure 13.

Here, we introduce the interactions of grain boundaries at a crystal/melt interface. The mechanisms behind the phenomena are not well understood yet, but we think

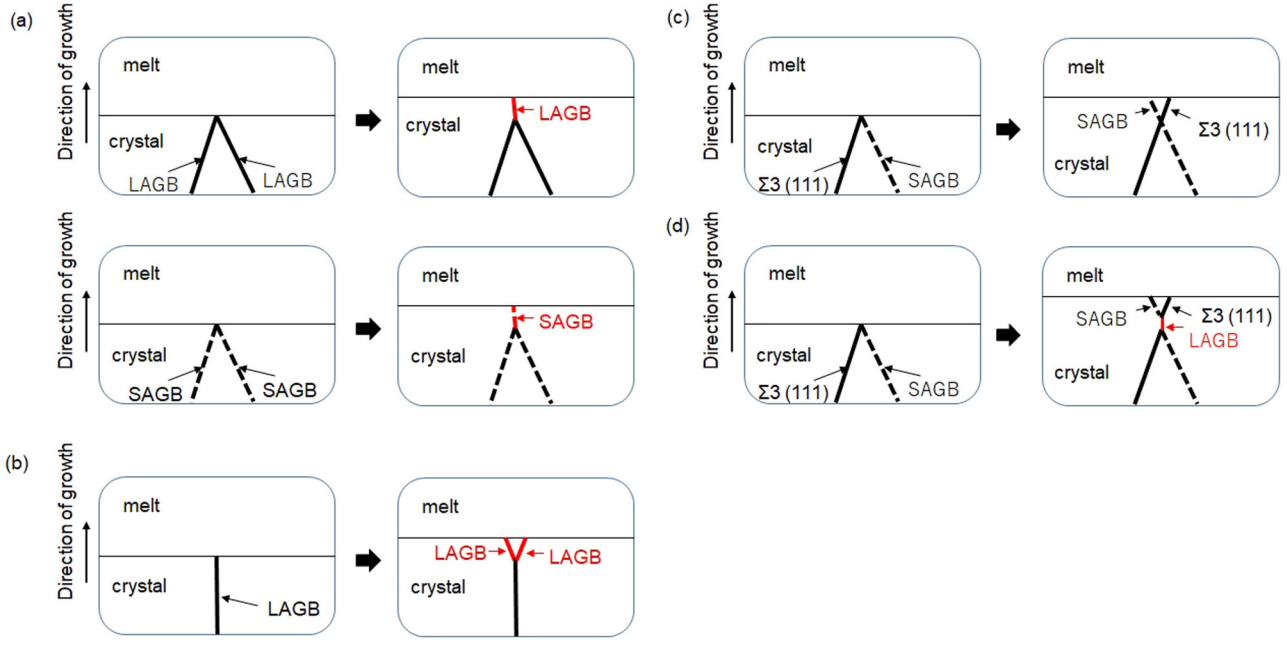

Figure 16: Summary of the observed interactions of grain boundaries at a crystal/melt interface: (a) two-grain boundaries produce a single grain boundary, (b) one grain boundary splits into two grain boundaries, (c) two grain boundaries penetrate each other, and (d) one grain boundary is formed after the impingement of two grain boundaries, but it splits into two grain boundaries immediately.

it is meaningful to show the observed phenomena for future study. Figure 14(a) and (b) show snapshots of the impingement of two-grain boundaries at the crystal/melt interface during directional solidification. In both cases, after the impingement of two large-angle grain boundaries (LAGB), one new LAGB was formed and extended with crystal growth. Such interactions of two-grain boundaries are often observed in mc-Si ingots [110,111]. Similarly, it was shown that the impingement of two SAGB produces one new SAGB [112]. On the contrary, cases in which one grain boundary decomposes into two-grain boundaries during growth were also observed [110,111,113].

The interaction between a SAGB and a Σ3 twin boundary was found to be different from those mentioned above [112,114]. Figure 15 shows the impingement of a SAGB and a Σ3 twin boundary [112]. At the impingement of these two boundaries at the crystal/melt interface (middle picture in Figure 15), they penetrate each other and continued to extend as seen in the image on the right in Figure 15. Such penetration of grain boundaries was not observed in the cases of impingement of two LAGBs or two SAGBs.

It was also shown that the behavior after the impingement of a SAGB and a Σ3 twin boundary was dependent on the misorientation angle of the SAGB before the impingement [114]. The patterns of grain boundary interactions observed to date are summarized in Figure 16 [110–114].

As shown above, the interaction of grain boundaries at a crystal/melt interface is complicated, and thus further studies are required to deepen our understanding. Not only experimental evidence but also theoretical and computational studies remain limited; thus, study of the dynamics of grain boundaries at the crystal/melt interface is an open topic for future studies.

4 Summary

It has been expected that the energy conversion efficiency of solar cells using mc-Si substrate will improve. For that to happen, control of the microstructure in mc-Si ingots in the directional solidification process is indispensable. Many phenomena occur at the crystal/melt interface whose mechanisms have not been clarified completely, especially regarding the dynamics of crystal defects, including grain boundaries, dislocations, and impurities. Observation of the macrostructures and microstructures of solidified mc-Si is of significance for indicating what takes place during directional solidification processes. In addition, global simulation and numerical analysis are also important for understanding the defect distributions in an entire ingot [115–123]. Transmission electron microscope (TEM) observations and various computational simulations have clarified the local distributions of defects [124–133]. *In situ* observation is also a powerful tool for obtaining direct evidence revealing phenomena at the crystal/melt interface. However, for clarification of crystal growth mechanisms, research from the theoretical side is also crucial.

Acknowledgments: The authors would like to thank Dr Masatoshi Tokairin, Dr Kuan-Kan Hu, Dr Xinbo Yang, and Mr Ryoichi Maeda for their efforts in some of the experiments. Also, the authors wish to express their thanks for fruitful discussions with Dr Haruhiko Morito and Dr Keiji Shiga.

Funding information: This study was funded by JSPS KAKENHI Grant numbers 16686001, 17656223, 18686060, 15KK0198, and 17H01336, and by the Cabinet Office, Government of Japan, through its "Funding Program for Next Generation World-Leading Researchers," GR016. Now this study is funded by JSPS KAKENHI Grant numbers 21H04658 and 21K20343.

Author contributions: Kozo Fujiwara: writing – original draft, writing – review and editing, methodology, formal analysis; Lu-Chung Chuang: writing – review, methodology, formal analysis; and Kensku Maeda: writing – review, methodology, formal analysis

Conflict of interest: There is no conflict of interest.

Data availability statement: The authors have a right to use graphics in this article.

References

[1] International Technology Roadmap for Photovoltaic (ITRPV), Results 2019, Eleventh Edition, April 2020.

[2] Ciszek, T. F., G. H. Schwuttke, and K. H. Yang. Solar-grade silicon by directional solidification in carbon crucibles. *IBM Journal of Research and Development*, Vol. 23, No. 3, 1979, pp. 270–277.

[3] Saito, T., A. Shimura, and S. Ichikawa. A reusable mold in directional solidification for silicon solar cells. *Solar Energy Materials*, Vol. 9, 1983, pp. 337–345.

[4] Ravishankar, P. S. Liquid encapsulated Bridgman (LEB) method for directional solidification of silicon using calcium chloride. *Journal of Crystal Growth*, Vol. 94, 1989, pp. 62–68.

[5] Kishore, R., J.-L. Pastol, and G. Revel. Growth and characterization of polycrystalline silicon ingots doped with Cu, C, B or Al by directional solidification for photovoltaic application. *Solar Energy Materials*, Vol. 19, 1989, pp. 221–236.

[6] Lee, G. H. and Z. H. Lee. Fabrication of polycrystalline Si wafer by vacuum casting and the effect of mold coating materials. *Journal of Crystal Growth*, Vol. 233, 2001, pp. 45–51.
[7] Ferrazza, F. Large size multicrystalline silicon ingots. *Solar Energy Materials & Solar Cells*, Vol. 72, 2002, pp. 77–81.
[8] Kim, J. M. and Y. K. Kim. Growth and characterization of 240 kg multicrystalline silicon ingot grown by directional solidification. *Solar Energy Materials & Solar Cells*, Vol. 81, 2004, pp. 217–224.
[9] Yang, D., D. Li, M. Ghosh, and H. J. Möller. Defects in nitrogen-doped multicrystalline silicon. *Physica B*, Vol. 344, 2004, pp. 1–4.
[10] Kvande, R., Ø. Mjøs, and B. Ryningen. Growth rate and impurity distribution in multicrystalline silicon for solar cells. *Materials Science and Engineering A*, Vol. 413–414, 2005, pp. 545–549.
[11] Nijs, J., S. Sivoththaman, J. Szlufcik, K. De Clercq, F. Duerinckx, E. Van Kerschaever, et al. Overview of solar cell technologies and results on high efficiency multicrystalline silicon substrates. *Solar Energy Materials and Solar Cells*, Vol. 48, 1997, pp. 199–217.
[12] O'mara, W. C., R. B. Herring, and L. P. Hunt, (eds.), *Handbook of semiconductor silicon technology*, Noyes Publications, Park Ridge, New Jersey, USA, 1990.
[13] Weidhaus, D., E. Schindlbeck, and K. Hesse. Trichlorosilane based silicon feedstock for the photovoltaic industry. *Silicon for the Chemical Industry VII*, Norway, 2004, pp. 189–200.
[14] Schindler, R. and A. Räuber. Defects in multicrystalline silicon. *Solid State Phenomena*, Vol. 19–20, 1991, pp. 341–352.
[15] Cuevas, A., M. Stocks, D. Macdonald, M. Kerr, and C. Samundsett. Recombination and trapping in multicrystalline silicon. *IEEE Transactions on Electron Devices*, Vol. 46, 1999, pp. 2026–2034.
[16] Barranco Díaz, M., W. Koch, C. Häßler, and H.-G. Bräutigam. Resistivity topography: a grain boundary characterisation method. *Solar Energy Materials & Solar Cells*, Vol. 72, 2002, pp. 473–486.
[17] Mudryi, A. V., A. I. Patuk, I. A. Shakin, A. G. Ulyashin, R. Job, W. R. Fahrner, et al. Impurities and defects in multicrystalline silicon for solar cells: low-temperature photoluminescence investigations. *Solar Energy Materials & Solar Cells*, Vol. 72, 2002, pp. 503–508.
[18] Kouteva-Arguirova, S., W. Seifert, M. Kittler, and J. Reif. Raman measurement of stress distribution in multicrystalline silicon materials. *Materials Science and Engineering*, Vol. B102, 2003, pp. 37–42.
[19] Chen, J., T. Sekiguchi, D. Yang, F. Yin, K. Kido, and S. Tsurekawa. Electron-beam-induced current study of grain boundaries in multicrystalline silicon. *Journal of Applied Physics*, Vol. 96, 2004, pp. 5490–5495.
[20] Chen, J., D. Yang, Z. Xi, and T. Sekiguchi. Recombination activity of Σ3 boundaries in boron-doped multicrystalline silicon: Influence of iron contamination. *Journal of Applied Physics*, Vol. 97, 2005, pp. 033701-1–033701-5.
[21] Tarasov, I., S. Ostapenko, K. Nakayashiki, and A. Rohatgi. Defect passivation in multicrystalline silicon for solar cells. *Applied Physics Letters*, Vol. 85, 2004, pp. 4346–4348.
[22] Buonassisi, T., A. A. Istratov, M. Heuer, M. A. Marcus, R. Jonczyk, J. Isenberg, et al. Synchrotron-based investigations of the nature and impact of iron contamination in multicrystalline silicon solar cells. *Journal of Applied Physics*, Vol. 97, 2005, pp. 074901-1–074901-11.
[23] Chen, J., T. Sekiguchi, R. Xie, P. Ahmet, T. Chikyo, D. Yang, et al. Electron-beam-induced current study of small-angle grain boundaries in multicrystalline silicon. *Scripta Materialia*, Vol. 52, 2005, pp. 1211–1215.
[24] Buonassisi, T., A. A. Istratov, M. D. Pickett, M. A. Marcus, T. F. Ciszek, and E. R. Weber. Metal precipitation at grain boundaries in silicon: Dependence on grain boundary character and dislocation decoration. *Applied Physics Letters*, Vol. 89, 2006, pp. 042102-1–042102-3.
[25] Acciarri, M., S. Binetti, A. Le Donne, S. Marchionna, M. Vimercati, J. Libal, et al. Effect of P-induced gettering on extended defects in n-type multicrystalline silicon. *Progress in Photovoltaics: Research and Applications*, Vol. 15, 2007, pp. 375–386.
[26] Lotnyk, A., J. Bauer, O. Breitenstein, and H. Blumtritt. A TEM study of SiC particles and filaments precipitated in multicrystalline Si for solar cells. *Solar Energy Materials & Solar Cells*, Vol. 92, 2008, pp. 1236–1240.
[27] Wang, H. Y., N. Usami, K. Fujiwara, K. Kutsukake, and K. Nakajima. Microstructures of Si multicrystals and their impact on minority carrier diffusion length. *Acta Materialia*, Vol. 57, 2009, pp. 3268–3276.
[28] Ganapati, V., S. Schoenfelder, S. Castellanos, S. Oener, R. Koepge, A. Sampson, et al. Infrared birefringence imaging of residual stress and bulk defects in multicrystalline silicon. *Journal of Applied Physics*, Vol. 108, 2010, pp. 063528-1–063528-13.
[29] Stokkan, G. Relationship between dislocation density and nucleation of multicrystalline silicon. *Acta Materialia*, Vol. 58, 2010, pp. 3223–3229.
[30] Gundel, P., M. C. Schubert, F. D. Heinz, W. Kwapil, W. Warta, G. Martinez-Criado, et al. Impact of stress on the recombination at metal precipitates in silicon. *Journal of Applied Physics*, Vol. 108, 2010, pp. 103707-1–103707-5.
[31] Ryningen, B., G. Stokkan, M. Kivambe, T. Ervik, and O. Lohne. Growth of dislocation clusters during directional solidification of multicrystalline silicon ingots. *Acta Materialia*, Vol. 59, 2011, pp. 7703–7710.
[32] Takahashi, I., N. Usami, H. Mizuseki, Y. Kawazoe, G. Stokkan, and K. Nakajima. Impact of type of crystal defects in multicrystalline Si on electrical properties and interaction with impurities. *Journal of Applied Physics*, Vol. 109, 2011, pp. 033504-1–033504-5.
[33] Wu, S., L. Wang, X. Li, P. Wang, D. Yang, D. You, et al. Influence of defects and impurities on the deteriorated border region in multicrystalline silicon ingots. *Crystal Research and Technology*, Vol. 47, 2012, pp. 7–12.
[34] Mankovics, D., R. P. Schmid, T. Arguirov, and M. Kittler. Dislocation-related photoluminescence imaging of mc-Si wafers at room temperature. *Crystal Research and Technology.*, Vol. 47, 2012, pp. 1148–1152.
[35] Käshammer, P. and T. Sinno. Interactions of twin boundaries with intrinsic point defects and carbon in silicon. *Journal of Applied Physics*, Vol. 114, 2013, pp. 083505-1–083505-11.
[36] Joonwichien, S., S. Matsushima, and N. Usami. Effects of crystal defects and their interactions with impurities on

electrical properties of multicrystalline Si. *Journal of Applied Physics*, Vol. 113, 2013, pp. 133503-1–133501-6.
[37] Oriwol, D., E.-R. Carl, A. N. Danilewsky, L. Syllar, W. Seifert, M. Kittler, et al. Small-angle subgrain boundaries emanating from dislocation pile-ups in multicrystalline silicon studied with synchrotron white-beam X-ray topography. *Acta Materialia*, Vol. 61, 2013, pp. 6903–6910.
[38] Schindler, F., B. Michl, J. Schön, W. Kwapil, W. Warta, and M. C. Schubert. Solar cell efficiency losses due to impurities from the crucible in multicrystalline silicon. *IEEE Journal of Photovoltaics*, Vol. 4, 2014, pp. 122–129.
[39] Autruffe, A., V. S. Hagen, L. Arnberg, and M. Di Sabatino. Dislocation generation at near-coincidence site lattice grain boundaries during silicon directional solidification. *Journal of Crystal Growth*, Vol. 411, 2015, pp. 12–18.
[40] Reimann, C., J. Friedrich, E. Meissner, D. Oriwol, and L. Sylla. Response of as grown dislocation structure to temperature and stress treatment in multi-crystalline silicon. *Acta Materialia*, Vol. 93, 2015, pp. 129–137.
[41] Mao, X., X. Yu, S. Yuan, and D. Yang. Recombination activity of sub-grain boundaries and dislocation arrays in quasi-single crystalline silicon. *Applied Physics Express*, Vol. 12, 2019, pp. 051012-1–051012-5.
[42] Ohno, Y., K. Tajima, K. Kutsukake, and N. Usami. Generation of dislocation clusters at triple junctions of random angle grain boundaries during cast growth of silicon ingots. *Applied Physics Express*, Vol. 13, 2020, pp. 105505-1–105505-4.
[43] Fujiwara, K., W. Pan, N. Usami, K. Sawada, M. Tokairin, Y. Nose, et al. Growth of structure-controlled polycrystalline silicon ingots for solar cells by casting. *Acta Materialia*, Vol. 54, 2006, pp. 3191–3197.
[44] Fujiwara, K., W. Pan, K. Sawada, M. Tokairin, N. Usami, Y. Nose, et al. Directional growth method to obtain high quality polycrystalline silicon from its melt. *Journal of Crystal Growth*, Vol. 292, 2006, pp. 282–285.
[45] Fujiwara, K., K. Maeda, N. Usami, G. Sazaki, Y. Nose, A. Nomura, et al. *In situ* observation of Si faceted dendrite growth from low-degree-of-undercooling melts. *Acta Materialia*, Vol. 56, 2008, pp. 2663–2668.
[46] Yang, X., K. Fujiwara, K. Maeda, J. Nozawa, H. Koizumi, and S. Uda. Dependence of Si faceted dendrite growth velocity on undercooling. *Applied Physics Letters*, Vol. 98, 2011, pp. 012113-1–012113-3.
[47] Stoddard, N., B. Wu, I. Witting, M. C. Wagener, Y. Park, G. A. Rozgonyi, et al. Casting single crystal silicon: Novel defect profiles from BP solar's mono$^{2\ TM}$ wafers. *Solid State Phenomena*, Vol. 131–133, 2008, pp. 1–8.
[48] Trempa, M., C. Reimann, J. Friedrich, G. Müller, and D. Oriwol. Mono-crystalline growth in directional solidification of silicon with different orientation and splitting of seed crystals. *Journal of Crystal Growth*, Vol. 351, 2012, pp. 131–140.
[49] Kutsukake, K., N. Usami, Y. Ohno, Y. Tokumoto, and I. Yonenaga. Mono-like silicon growth using functional grain boundaries to limit area of multicrystalline grains. *IEEE Journal of Photovoltaics*, Vol. 4, 2014, pp. 84–87.
[50] Iwata, T., I. Takahashi, and N. Usami. Effects of grain boundary structure controlled by artificially designed seeds on dislocation generation. *Japanese Journal of Applied Physics*, Vol. 56, 2017, pp. 075501-1–075501-4.
[51] Zhang, F., X. Yu, C. Liu, S. Yuan, X. Zhu, Z. Zhang, et al. Designing functional Σ13 grain boundaries at seed junctions for high-quality cast quasi-single crystalline silicon. *Solar Energy Materials and Solar Cells*, Vol. 200, 2019, pp. 109985-1–109985-7.
[52] Nose, Y., I. Takahiashi, W. Pan, N. Usami, K. Fujiwara, and K. Nakajima. Floating cast method to realize high-quality Si bulk multicrystals for solar cells. *Journal of Crystal Growth*, Vol. 311, pp. 228–231.
[53] Nakajima, K., R. Murai, K. Morishita, K. Kutsukake, and N. Usami. Growth of multicrystalline Si ingots using non-contact crucible method for reduction of stress. *Journal of Crystal Growth*, Vol. 344, 2012, pp. 6–11.
[54] Nakajima, K., M. Nakanishi, M. Su, and C. Hsu. Theoretical distributions of point-defect concentration in a Si ingot grown inside a malt using the noncontact crucible method considering accumulation effect of diffusion flux. *Journal of Crystal Growth*, Vol. 547, 2020, pp. 125810-1–125810-9.
[55] Wong, Y. T., C. Hsu, and C. W. Lan. Development of grain structures of multi-crystalline silicon from randomly oriented seeds in directional solidification. *Journal of Crystal Growth*, Vol. 387, 2014, pp. 10–15.
[56] Yang, Y. M., A. Yu, B. Hsu, W. C. Hsu, A. Yang, and C. W. Lan. Development of high-performance multicrystalline silicon for photovoltaic industry. *Progress in Photovoltaics: Research and Applications*, Vol. 23, 2015, pp. 340–351.
[57] Lan, C. W., C. F. Yang, A. Lan, M. Yang, A. Yu, H. P. Hsu, et al. Engineering silicon crystals for photovoltaics. *CrystEngComm*, Vol. 18, 2016, pp. 1474–1485.
[58] Schwanke, S., M. Trempa, C. Reimann, M. Kuczynski, G. Schroll, J. Sans, et al. Production of high performance multi-crystalline silicon ingots for PV application by using contamination-free SixNy seed particles. *Journal of Crystal Growth*, Vol. 522, 2019, pp. 151–159.
[59] Lei, Q., L. He, S. Rao, C. Tang, L. Ming, Y. Xu, et al. Production of high performance multi-crystalline silicon ingot by using composite nucleant. *Journal of Crystal Growth*, Vol. 542, 2020, pp. 125666-1–125666-6.
[60] Wang, P., C. Cui, D. Yang, and X. Yu. Seed-assisted growth of cast-mono silicon for photovoltaic application: Challenges and strategies. *Solar PRL*, Vol. 4, 2020, pp. 1900486-1–1900486-20.
[61] Fujiwara, K., K. Nakajima, T. Ujihara, N. Usami, G. Sazaki, H. Hasegawa, et al. *In situ* observations of crystal growth behavior of silicon melt. *Journal of Crystal Growth*, Vol. 243, 2002, pp. 275–282.
[62] Chikawa, H., H. Shibata, T. Emi, and M. Suzuki. "In-situ" real time observation of planar to cellular and cellular to dendritic transition of crystals growing in Fe-C alloy melts. *Materials Transactions, JIM*, Vol. 37, 1996, pp. 620–626.
[63] Nakajima, K. and S. Mizoguchi. Capillary interaction between inclusion particles on the 16Cr stainless steel melt surface. *Metallurgical and Materials Transactions B*, Vol. 32B, 2001, pp. 629–641.
[64] Fujiwara, K., Y. Obinata, T. Ujihara, N. Usami, G. Sazaki, and K. Nakajima. In-situ observations of melt growth behavior of polycrystalline silicon. *Journal of Crystal Growth*, Vol. 15, 2004, pp. 124–129.
[65] Fujiwara, K., Y. Obinata, T. Ujihara, N. Usami, G. Sazaki, and K. Nakajima. Grain growth behaviors of polycrystalline

silicon during melt growth processes. *Journal of Crystal Growth*, Vol. 266, 2004, pp. 441–448.

[66] Tandjaoui, A., N. Mangelinck-Noël, G. Reinhart, J.-J. Furter, B. Billia, T. Lafford, et al. Real time observation of the directional solidification of multicrystalline silicon: X-ray imaging characterization. *Energy Procedia*, Vol. 27, 2012, pp. 82–87.

[67] Tandjaoui, A., N. Mangelinck-Noël, G. Reinhart, B. Billia, and X. Guichard. Twinning occurrence and grain competition in multi-crystalline silicon during solidification. *Comptes Rendus Physique*, Vol. 14, 2013, pp. 141–148.

[68] Tsoutsouva, M. G., V. A. Oliveira, D. Camel, J. Baruchel, B. Marie, and T. A. Lafford. Mono-like silicon ingots grown on low angle misoriented seeds: Defect characterization by synchrotron X-ray diffraction imaging. *Acta Materialia*, Vol. 88, 2015, pp. 112–120.

[69] Ouaddah, H., I. Périchaud, D. Barakel, O. Palais, M. Di Sabatino, G. Reinhart, et al. Role of impurities in silicon solidification and electrical properties studied by complementary *in situ* and ex situ methods. *Physica Status Solidi A*, Vol. 216, 2019, pp. 1900298-1–1900298-10.

[70] Ouaddah, H., M. Becker, T. Riberi-Béridot, M. Tsoutsouva, V. Stamelou, G. Regula, et al. X-ray based *in situ* investigation of silicon growth mechanism dynamics-Application to grain and defect formation. *Crystals*, Vol. 10, 2020, pp. 555-1–555-25.

[71] Wulff, G. Zur Frage der Geschwindigkeit des Wachstums und der Auflösung der Krystallflagen. *Zeitschrift Fur Kristallographie*, Vol. 34, 1901, pp. 449–530.

[72] Laue, M. V. Der Wulffsche Satz für die Gleichgewichtsform von Kristallen. *Zeitschrift für Kristallographie - Crystalline Materials*, Vol. 105, 1944, pp. 124–133.

[73] Yang, X., K. Fujiwara, K. Maeda, J. Nozawa, H. Koizumi, and S. Uda. Crystal growth and equilibrium crystal shapes of silicon in the melt. *Progress in Photovoltaics: Research and Applications*, Vol. 22, 2014, pp. 574–580.

[74] Barinovs, G., A. Sabanskis, and A. Muiznieks. Study of silicon crystal surface formation based on molecular dynamics simulation results. *Journal of Crystal Growth*, Vol. 391, 2014, pp. 13–17.

[75] Miller, W. and A. Popescu. Micro structures in the grain evolution during solidification of silicon: Phase field calculations. *Acta Materialia*, Vol. 140, 2017, pp. 1–9.

[76] Boukellal, A. K., A. K. S. Elvalli, and J.-M. Debierre. Equilibrium and growth facetted shapes in isothermal solidification of silicon: 3D phase-field simulations. *Journal of Crystal Growth*, Vol. 522, 2019, pp. 37–44.

[77] Fujiwara, K., K. Maeda, H. Koizumi, J. Nozawa, and S. Uda. Effect of silicon/crucible interfacial energy on orientation of multicrystalline silicon ingot in unidirectional growth. *Journal of Applied Physics*, Vol. 112, 2012, pp. 113521-1–113521-5.

[78] Nagashio, K. and K. Kuribayashi. Growth mechanism of twin-related and twin-free facet Si dendrites. *Acta Materialia*, Vol. 53, 2005, pp. 3021–3029.

[79] Fujiwara, K., K. Maeda, N. Usami, G. Sazaki, Y. Nose, and K. Nakajima. Formation mechanism of parallel twins related to Si-faceted dendrite growth. *Scripta Materialia*, Vol. 57, 2007, pp. 81–84.

[80] Fujiwara, K., K. Maeda, N. Usami, and K. Nakajima. Growth mechanism of Si-faceted dendrites. *Physical Review Letters*, Vol. 101, 2008, pp. 055503-1–055503-4.

[81] Fujiwara, K. Crystal growth behaviors of silicon during melt growth processes. *International Journal of Photoenergy*, Vol. 2012, 2012, pp. 169829-1–169829-16.

[82] Shiga, K., M. Kawano, K. Maeda, H. Morito, and K. Fujiwara. The *in situ* observation of faceted dendrite growth during the directional solidification of GaSb. *Scripta Materialia*, Vol. 168, 2019, pp. 56–60.

[83] Miyazawa, H., L. Liu, and K. Kakimoto. Numerical analysis of influence of crucible shape on interface shape in a unidirectional solidification process. *Journal of Crystal Growth*, Vol. 310, 2008, pp. 1142–1147.

[84] Wu, B., N. Stoddard, R. Ma, and R. Clark. Bulk multicrystalline silicon growth for photovoltaic (PV) application. *Journal of Crystal Growth*, Vol. 310, 2008, pp. 2178–2184.

[85] Wei, J., H. Zhang, L. Zheng, C. Wang, and B. Zhao. Modeling and improvement of silicon ingot directional solidification for industrial production system. *Solar Energy Materials & Solar Cells*, Vol. 93, 2009, pp. 1531–1539.

[86] Popescu, A. and D. Vizman. Numerical study of melt convection and interface shape in a pilot furnace for unidirectional solidification of multicrystalline silicon. *Crystal Growth & Design*, Vol. 12, 2012, pp. 320–325.

[87] Dadzis, K., D. Vizman, and J. Friedrich. Unsteady coupled 3D calculations of melt flow, interface shape, and species transport for directional solidification of silicon in a traveling magnetic field. *Journal of Crystal Growth*, Vol. 367, 2013, pp. 77–87.

[88] Dropka, N. and M. Holena. Optimization of magnetically driven directional solidification of silicon using artificial neural networks and Gaussian process models. *Journal of Crystal Growth*, Vol. 471, 2017, pp. 53–61.

[89] Zhang, Z., X. Yu, S. Yuan, and D. Yang. Experimental study of 3D solid-liquid interfaces and their influence on directional solidification silicon ingot. *Solar Energy Materials & Solar Cells*, Vol. 224, 2021, pp. 110991-1–110991-7.

[90] Tokairin, M., K. Fujiwara, K. Kutsukake, N. Usami, and K. Nakajima. Formation mechanism of a faceted interface: *In situ* observation of the Si (100) crystal-melt interface during crystal growth. *Physical Review B*, Vol. 80, 2009, pp. 174108-1–174108-4.

[91] Tokairin, M., K. Fujiwara, K. Kutsukake, H. Kodama, N. Usami, and K. Nakajima. Pattern formation mechanism of a periodically faceted interface during crystallization of Si. *Journal of Crystal Growth*, Vol. 312, 2010, pp. 3670–3674.

[92] Fujiwara, K., R. Gotoh, X. Yang, H. Koizumi, J. Nozawa, and S. Uda. Morphological transformation of a crystal-melt interface during unidirectional growth of silicon. *Acta Materialia*, Vol. 59, 2011, pp. 4700–4708.

[93] Jackson, K. A. Mechanism of growth. *Liquid metals and solidification*, American Society for Metals, Cleveland, Ohio, 1958, pp. 174–186.

[94] Jackson, K. A. Interface structure. *Growth and perfection of crsytals*, R. H. Dovemus, Roberts, B. W., Turnbull, D., edited by, Wiley, New York, 1958, pp. 319–324.

[95] Mullins, W. W. and R. F. Sekerka. Stability of a planar interface during solidification of a dilute binary alloy. *Journal of Applied Physics*, Vol. 35, pp. 444–451.

[96] Yi, K.-W., H.-T. Chung, H.-W. Lee, and J.-K. Yoon. The effects of pulling rates on the shape of crystal/melt interface in Si single crystal growth by the Czochralski method. *Journal of Crystal Growth*, Vol. 132, 1993, pp. 451–460.
[97] Hu, K.-K., K. Maeda, K. Shiga, H. Morito, and K. Fujiwara. The effect of grain boundaries on instability at the crystal/melt interface during the unidirectional growth of Si. *Materialia*, Vol. 7, 2019, pp. 100386-1–100386-9.
[98] Nishioka, S., H. Kuriyaki, and K. Hirakawa. Influence of crystallinity on the electrical property of KFe(S1-xSex)2. *Japanese Journal of Applied Physics*, Vol. 35, 1996, pp. 648–651.
[99] Duffar, T. and A. Nadri. On the twinning occurrence in bulk semiconductor crystal growth. *Scripta Materialia*, Vol. 62, 2010, pp. 955–960.
[100] Fujiwara, K., M. Ishii, K. Maeda, H. Koizumi, J. Nozawa, and S. Uda. The effect of grain boundary characteristics on the morphology of the crystal/melt interface of multicrystalline silicon. *Scripta Materialia*, Vol. 69, 2013, pp. 266–269.
[101] Tsoutsouva, M. G., T. Ronero-Béridot, G. Regula, G. Reinhart, J. Baruchel, F. Guittonneau, et al. *In situ* investigation of the structural defect generation and evolution during the directional solidification of <110> seeded growth Si. *Acta Materialia*, Vol. 115, 2016, pp. 210–223.
[102] Fujiwara, K., R. Maeda, K. Maeda, and H. Morito. *In situ* observation of twin boundary formation at grain boundary groove during directional solidification of Si. *Scripta Materialia*, Vol. 133, 2017, pp. 62–69.
[103] Lin, H. K. and C. W. Lan. Revisiting the twinning mechanism in directional solidification of multi-crystalline silicon sheet. *Acta Materialia*, Vol. 131, 2017, pp. 1–10.
[104] Lin, H. K. and C. W. Lan. A multilayer nucleation model for twinning during directional solidification of multi-crystalline silicon. *Journal of Crystal Growth*, Vol. 478, 2017, pp. 47–51.
[105] Duffar, T. and A. Nadri. The grain-grain-liquid triple phase line during solidification of multi-crystalline silicon. *Comptes Rendus Physique*, Vol. 14, 2013, pp. 185–191.
[106] Tandjaoui, A., N. Mangelinck-Noel, G. Reinhart, B. Billia, T. Lafford, and J. Baruchel. Investigation of grain boundary grooves at the solid-liquid interface during directional solidification of multi-crystalline silicon: *in situ* characterization by X-ray imaging. *Journal of Crystal Growth*, Vol. 377, 2013, pp. 203–211.
[107] Hu, K.-K., K. Maeda, H. Morito, K. Shiga, and K. Fujiwara. *In situ* observation of grain-boundary development from a facet-facet groove during solidification of silicon. *Acta Materialia*, Vol. 153, 2018, pp. 186–192.
[108] Chuang, L.-C., K. Maeda, H. Morito, K. Shiga, and K. Fujiwara. Origin of small-angle grain boundaries during directional solidification in multicrystalline silicon. *Materialia*, Vol. 3, 2018, pp. 347–352.
[109] Chuang, L.-C., T. Kiguchi, Y. Kodama, K. Maeda, K. Shiga, H. Morito, et al. Influence of interfacial structure on propagating direction of small-angle grain boundaries during directional solidification of multicrystalline silicon. *Scripta Materialia*, Vol. 172, pp. 105–109.
[110] Pralash, R. R., K. Jiptner, J. Chen, Y. Miyajima, H. Harada, and T. Sekiguchi. Grain boundary interactions in multicrystalline silicon grown from small randomly oriented seeds. *Applied Physics Express*, Vol. 8, 2015, pp. 035502-1–035502-4.
[111] Lin, H. K., M. C. Wu, C. C. Chen, and C. W. Lan. Evolution of grain structures during directional solidification of silicon wafers. *Journal of Crystal Growth*, Vol. 439, 2016, pp. 40–46.
[112] Chuang, L.-C., K. Maeda, H. Morito, K. Shiga, W. Miller, and K. Fujiwara. *In situ* observation of interaction between grain boundaries during directional solidification of Si. *Scripta Materialia*, Vol. 148, 2018, pp. 37–41.
[113] Chuang, L.-C., K. Maeda, K. Shiga, H. Morito, and K. Fujiwara. A {112}Σ3 grain boundary generated from the decomposition of a Σ9 grain boundary in multicrystalline silicon during directional solidification. *Scripta Materialia*, Vol. 167, 2019, pp. 46–50.
[114] Chuang, L.-C., K. Maeda, H. Morito, K. Shiga, W. Miller, and K. Fujiwara. Effect of misorientation angle of grain boundary on the interaction with Σ3 boundary at crystal/melt interface of multicrystalline silicon. *Materialia*, Vol. 7, 2019, pp. 100357-1–100357-10.
[115] Matsuo, H. R. B., S. Ganesh, L. Nakano, Y. Liu, K. Kangawa, Y. Arafune, et al. Thermodynamical analysis of oxygen incorporation from a quartz crucible during solidification of multicrystalline silicon for solar cell. *Journal of Crystal Growth*, Vol. 310, 2008, pp. 4666–4671.
[116] Gao, B., S. Nakano, and K. Kakimoto. Global simulation of coupled carbon and oxygen transport in a unidirectional solidification furnace for solar cells. *Journal of The Electrochemical Society*, Vol. 157, 2010, pp. H153–H159.
[117] Reimann, C., M. Trempa, T. Jung, J. Friedrich, and G. Müller. Modeling of incorporation of O, N, C and formation of related precipitates during directional solidification of silicon under consideration of variable processing parameters. *Journal of Crystal Growth*, Vol. 312, 2010, pp. 858–885.
[118] Gao, B., S. Nakano, and K. Kakimoto. Influence of reaction between silica crucible and graphite susceptor on impurities of multicrystalline silicon in a unidirectional solidification furnace. *Journal of Crystal Growth*, Vol. 314, 2010, pp. 239–245.
[119] Zheng, L., X. Ma, D. Hu, H. Zhang, T. Zhang, and Y. Wan. Mechanism and modeling of silicon carbide formation and engulfment in industrial silicon directional solidification growth. *Journal of Crystal Growth*, Vol. 318, 2011, pp. 313–317.
[120] Bellmann, M. P., B. Panjwani, M. Syvertsen, and E. A. Meese. Dynamic simulation of impurity transport and chemical reactions in a Bridgman furnace for directional solidification of multi-crystalline silicon. *Journal of Crystal Growth*, Vol. 369, 2013, pp. 47–54.
[121] Simons, P., A. Lankhorst, A. Habraken, A.-J. Faber, D. Tiuleanu, and R. Pingel. Validation of a 3D multi-physics model for unidirectional silicon solidification. *Journal of Crystal Growth*, Vol. 340, 2012, pp. 102–111.
[122] Fang, H., Q. Zhang, Y. Pan, S. Wang, N. Zhou, L. Zhou, et al. Characteristics of thermal stress evolution during the cooling stage of multicrystalline silicon. *Journal of Thermal Stresses*, Vol. 36, 2013, pp. 947–961.
[123] Avinash Kumar, M., G. Aravindan, M. Srinivasan, and P. Ramasamy. Comparative analysis of thermal stress induced dislocations in 7 kg, 40 kg and 330 kg multi-crystalline silicon ingots grown by directional solidification. *Journal of Crystal Growth*, Vol. 550, 2020, pp. 125901-1–125901-9.

[124] Seibt, M., H. Hedemann, A. A. Istratov, F. Riedel, A. Sattler, and W. Schröter. Structural and electrical properties of metal silicide precipitates in silicon. *Physica Status Solidi* (*a*), Vol. 171, 1999, pp. 301–310.

[125] Käshammer, P. and T. Sinno. A mechanistic study of impurity segregation at silicon grain boundaries. *Journal of Applied Physics*, Vol. 118, 2015, pp. 095301-1–095301-11.

[126] Ohno, Y. K., K. Inoue, M. Kutsukake, T. Deura, I. Ohsawa, H. Yonenaga, et al. Nanoscopic mechanism of Cu precipitation at small-angle tilt boundaries in Si. *Physical Review B*, Vol. 91, 2015, pp. 235315-1–235315-5.

[127] Ohno, Y., K. Kutsukake, M. Deura, I. Yonenaga, Y. Shimizu, M. Ebisawa, et al. Recombination activity of nickel, copper, and oxygen atoms segregating at grain boundaries in mono-like silicon crystals. *Applied Physics Letters*, Vol. 109, 2016, pp. 142105-1–142105-4.

[128] Oriwol, D., M. Trempa, L. Sylla, and H. S. Leipner. Investigation of dislocation cluster evolution during directional solidification of multicrystalline silicon. *Journal of Crystal Growth*, Vol. 463, 2017, pp. 1–9.

[129] Zhou, N., X. Wei, and L. Zhou. Formation of dislocations in the growth of silicon along different crystallographic directions – A molecular dynamics study. *Crystals*, Vol. 8, 2018, pp. 346-1–3467.

[130] Zhou, N., X. Sui, X. He, S. Huang, and L. Zhou. Nucleation of self-growth dislocations on growth front during the solidification process of silicon. *Journal of Applied Physics*, Vol. 125, 2019, pp. 155108-1–155108-6.

[131] Zhao, D. and Y. Li. Revealing the factors influencing grain boundary segregation of P, As in Si: Insights from first-principles. *Acta Materialia*, Vol. 168, 2019, pp. 52–62.

[132] Ohno, Y., J. Ren, S. Tanaka, M. Kohyama, K. Inoue, Y. Shimizu, et al. Insight into segregation sites for oxygen impurities at grain boundaries in silicon. *Applied Physics Express*, Vol. 14, 2021, pp. 041003-1–041003-4.

[133] Ohno, Y., T. Yokoi, Y. Shimizu, J. Ren, K. Inoue, Y. Nagai, et al. Segregation mechanism of arsenic dopants at grain boundaries in silicon. *Science and Technology of Advanced Materials: Methods*, Vol. 1, pp. 169–180.